Autonomous Satellite System Synchronization Schemes via Optical Two-Way Time Transfer and Distributed Composite Clock

Christian Trainotti, Manuele Dassié, Gabriele Giorgi, *German Aerospace Center (DLR)*
Amir Khodabandeh, *Department of Infrastructure Engineering, The University of Melbourne*
Christoph Günther, *German Aerospace Center (DLR) and Technical University of Munich (TUM)*

Biographies

Christian Trainotti received a M.Sc. in mechanical engineering from the Technical University of Munich, Germany and a M.Sc. in mechatronic engineering from the University of Trento, Italy. Since 2018 he works at the Institute of Communications and Navigation at the German Aerospace Center (DLR) on precise and robust time generation for GNSS applications.

Manuele Dassié holds a B.Sc in Physics from the University of Fribourg, Switzerland and a M.Sc in Aerospace Engineering from Institut Supérieur de l'Aéronautique et de l'Espace in Toulouse, France. Currently, Manuele is working on the synchronization of satellites at system level and on the implementation of a GNSS simulator, at the DLR-KN Institute.

Gabriele Giorgi is a researcher and team lead at the Institute of Communications and Navigation, German Aerospace Center (DLR). He obtained his doctorate following his work on Global Navigation Satellite System (GNSS)-based attitude determination from the Delft University of Technology, the Netherlands. His main research focuses on system and processing architectures for next-gen GNSSs, high-precision navigation, orbit determination, visual navigation and multi-sensor fusion.

Amir Khodabandeh is a lecturer at the Department of Infrastructure Engineering, the University of Melbourne, Melbourne, Australia. He is also an Alexander von Humboldt research fellow at DLR. His research interests include geodetic estimation theory, interferometric positioning, and GNSS quality control.

Christoph Günther studied theoretical physics at the Swiss Federal Institute of Technology (ETH) in Zurich. He completed his PhD in 1984 and worked in different industrial positions at Asea Brown Boveri, Ascom and Ericsson. Since 2003, he is the director of the Institute of Communications and Navigation at the German Aerospace Center (DLR), and since 2004 he is additionally holding the Chair of Communications and Navigation at Technical University of Munich (TUM).

Abstract
To improve the provision of a global satellite navigation service, the German Aerospace Center (DLR) - Institute of Communication and Navigation - is proposing a next-generation global navigation satellite architecture named Kepler. Autonomous synchronization at picosecond-level is a fundamental component of the Kepler concept, achieved via two-way time transfer (TWTT) schemes enabled by optical inter-satellite links (OISLs). This level of synchronization is only achievable if relativistic effects are adequately considered. In this paper we present the synchronization scheme for Kepler: all satellites perform pairwise relativistic TWTT, providing relative clock offsets in a predefined coordinate time scale. These are then distributed across the whole constellation and are used as input for a space-based distributed clock ensemble. Each satellite realizes a local copy of the Kepler system time (KST) by steering a local oscillator, so that all satellites will tend to "beat" the same time, thus achieving a tight synchronization. We show how measurement noise impacts the final synchronization level, in two different designs of the Kepler architecture. Additionally, the impact of constant biases on the system time generation is analyzed. Finally, we assess the impact of the choice of constellation's measurement topologies (open versus closed rings). The synchronization performance is expressed in terms of maximum time offset between any two satellites of the constellation.

1. INTRODUCTION

In recent years, the space sector has seen an increased interest in optical communications for ground-to-satellite and inter-satellite links. Such a technology in future global navigation satellite systems (GNSSs) can greatly improve the navigation and time dissemination services. The German Aerospace Center (DLR) is active in the design and development of a next-generation GNSS architecture, named Kepler, in which satellites are equipped with optical terminals for intra-system time-transfer, optical ranging and communication. The system consists of a constellation of optically-linked satellites in Medium Earth Orbit (MEO), possibly with a complementary constellation of satellites in Low Earth Orbit (LEO). The latter would support the system with system calibration and signal monitoring, and aid the precise orbit determination (POD) of MEO satellites (Günther, 2018; Michalak et al., 2021).

In the Kepler architecture, Optical Inter-Satellite Links (OISLs) are used to perform time transfer between satellites at the picosecond level. This in turn allows inter-satellite ranging with sub-millimeter precision. POD performance will largely benefit from the additional ranging observables, with a significant improvement in Signal-in-Space Range Error (SiSRE) (Michalak et. al, 2021). By leveraging OISLs, the Kepler architecture combines a tight constellation synchronization with enhanced POD capabilities, thus broadcasting higher quality orbital parameters to the final user without the need for a-posteriori corrections.

Another benefit of OISLs is the autonomy and resiliency of the system: in principle, only a small set of ground stations is sufficient to guarantee orbit determination at centimeter-level, while maintaining observability of the Earth Rotation Parameters (Michalak et. al, 2021). In the extreme case of complete absence of any ground infrastructure, the system can potentially still be used as a "space clock" where a highly stable time scale is generated from the ensemble of all satellite clocks. Such a time scale would be less affected by terrestrial phenomena, e.g. the poor knowledge of the geopotential on the surface of Earth (Wolf & Petit, 1995).

With spacecrafts pair-wise connected with two-way coherent laser links, coherent transceivers allow the generation and reception of timestamps with sub-picosecond precision, enabling the exchange of measured time-of-arrival information between the paired satellites. Two-Way Time Transfer (TWTT) methods make it possible to retrieve clock offsets with picosecond-level accuracy (Poliak et al. 2018; Calvo et al. 2020; Surof et al. 2019,2022). All the relative clock offsets are then distributed through the whole constellation and used as input of the synchronization algorithm based on the concept of clock ensembling, where each satellite generates a local copy of the ensemble time. As shown in the following, the local timescale realizations are synchronized at picosecond-level, enabling the provision of a stable system time common to all satellites. Finally, the link with terrestrial time scales, such as Coordinated Universal Time (UTC), can be ensured in two ways: either by estimation of the offset between the "space clock" and the reference terrestrial time scale performed with conventional methods, or by one or more optical exchanges between a satellite of the Kepler constellation and one ground station.

Relativistic effects are significant when compared to the time deviation of the clocks considered in the Kepler system, and to the synchronization capabilities offered by the OISLs. Satellites' relative velocities and gravitational fields in the near-Earth region give both origin to location-dependent readings of the frequency and time generated by the satellite clocks. These relativistic effects include Doppler shifts due to relative velocity differentials, gravitational frequency shifts, and other effects on the propagation of light in a curved spacetime. If such effects are not properly accounted for, relativistic biases will jeopardize the synchronization system (Ashby, 2003). In a previous work (Dassié & Giorgi, 2021), we presented and analyzed a relativistic two-way synchronization scheme based on the exchange of time stamps via optical signals, which allows estimating the offset between two satellite clocks with respect to a defined coordinate time scale. The model therein guarantees a time transfer at picosecond-level.

In this paper we extend the synchronization scheme to a constellation of N satellites equipped with clocks of various types. System synchronization can be achieved from a "cold-start" without prior synchronization in two consecutive steps: a first step is required to perform a non-relativistic coarse synchronization to align all satellite clocks (in a coordinate time scale) within a few tens of microseconds. This step mitigates errors in the subsequent relativistic correction induced by uncertainties in the satellite position and velocity. Then, at predetermined intervals, all satellites perform pairwise relativistic time transfer. The result of these exchanges are relative offsets in coordinate time that are distributed via OISLs across the whole constellation. The Kepler System Time (KST) is then realized by means of a space-based distributed clock ensemble, comprising all satellite clocks. Each satellite runs the same ensembling algorithm based on the same set of distributed clock offsets, thus realizing a local copy of the KST. The ensembling algorithm consists of a Kalman filter and a feedback loop steering a local oscillator to the KST, which is a weighted average of the contributions of all the clocks participating in the ensemble. By having a local oscillator steered to the KST, all satellites will "beat" the same time, thus achieving a tight synchronization.

2. RELATIVE CLOCK OFFSET DETERMINATION

2.1 SIMULTANEITY

The theory of relativity refutes the notions of absolute and independent space and time, resulting in different time rates in different reference systems (RSs). As a consequence, the notion of simultaneity loses its absolute and unique meaning.

To address the problem of relativistic synchronization it is first necessary to introduce the concepts of proper and coordinate quantities. Proper quantities are the direct results of observations without any information that depends on the choice of a spacetime reference frame. In this paper, the most fundamental quantity is the proper time: the physical, local output of an ideal clock located in a frame of reference that is attached to the observer itself (proper to that observer). Coordinate quantities are instead dependent on the choice of a spacetime coordinate system. An example is the coordinate time difference between two events (the difference between the time coordinates of these events) or the rate of a clock with respect to the coordinate time of some spacetime RS, which are both dependent on the chosen RS (Petit & Wolf, 2005).

To characterize inter-satellite synchronization we adopt here the concept of simultaneity exposed in Klioner (1992): consider two events fixed in some RS by the values of their 4-dimensional coordinates $E_1 = (t_1, x_1, y_1, z_1)$ and $E_2 = (t_2, x_2, y_2, z_2)$. The time scale t is the coordinate time, which coincides with the proper time scale that an observer at rest in the RS uses to define the space-time coordinates. The events E_1 and E_2 are considered to be simultaneous with respect to this RS if their values of time coordinate are equal: $t_1 = t_2$. This definition of simultaneity is called "coordinate simultaneity". The definition of synchronization arises naturally from the concept of simultaneity, as synchronized clocks beat the same time markers simultaneously. When addressing synchronization, we must bear in mind that we are dealing with coordinate synchronization, where clocks could be synchronized when observed by the coordinate RS, but could beat asynchronously when observed by a different RS. In our specific case, the chosen coordinate RS is a realization of a local inertial frame, or Earth Center Inertial (ECI) coordinate system. The coordinate time t of this ECI frame is defined at infinity, outside Earth's gravity well (Ashby, 2003).

During the initialization of the Kepler system, all satellite clocks tick at a different rate with respect to the coordinate time t. Furthermore, as the clocks are not yet "coordinate synchronized" from the point of view of an observer in the coordinate ECI frame, they present a relative offset. This offset is the quantity that we want to either determine or force to zero, to achieve synchronization of the satellites' clocks.

Our approach to relativistic synchronization is divided in sequential steps: first, the proper timestamps of clocks are transformed into coordinate timestamps via a relativistic transformation; then, a dynamic TWTT is performed in order to determine the relative coordinate offset between each pair of clocks; finally, this information is distributed to the whole constellation, a composite clock is computed on each satellite, and a correction is derived and applied to the local oscillator to realize a local copy of the system time.

2.2 TIMESTAMPS TRANSFORMATION

The relationship between the proper time τ of a clock in the vicinity of Earth's center (orbiting the planet or on its surface) and the coordinate time t can be derived from the spacetime metric, which describes the relation between spatial and time coordinates. This metric is derived from the metric tensor, the solution of the Einstein Field Equation. The Field Equation links the curvature of spacetime to the density and flow of matter and energy at a certain point in the universe. When Earth is modelled as a non-rotating spherical mass, the solution of such equation leads to the Schwarzschild metric (Schutz, 2009). Consider a clock located at spatiotemporal coordinates $\boldsymbol{r} = (t, r, \theta, \phi)$, which are the spherical ECI coordinates and t is the coordinate time of the ECI frame. From the Schwarzschild metric one can derive the rate of such clock with respect to coordinate time t (Ashby, 2003):

$$\frac{d\tau}{dt} \approx 1 + \frac{V(\boldsymbol{r})}{c^2} - \frac{v^2}{2c^2} \tag{1}$$

where c is the speed of light, $V(\boldsymbol{r})$ is the gravitational potential at position $\boldsymbol{r}$ and v is the clock's velocity expressed in ECI coordinates. In principle $V(\boldsymbol{r})$ should include the contribution of Earth's gravitational potential (geopotential) as well as the gravitational contribution of the other celestial bodies in the solar system. In the specific case of MEO and LEO satellites, all bodies other than Earth account for much less than picosecond per second and can be neglected. Nonetheless, the geopotential has to be expressed as a sum of multipole terms up to the third order (Dassié & Giorgi, 2021).

The proper timestamps are transformed into coordinate timestamps via integration of (1):

$$t(\tau) = t_0 + \int_{\tau_0}^{\tau} \left(\frac{d\tau}{dt}\right)^{-1} d\tau \tag{2}$$

The lower bound of the integral τ_0 and the constant $t_0 = t(\tau_0)$ on the right side of (2) can be arbitrarily chosen on each satellite. The choice of different initial conditions leads to the transformation of the same proper time scale τ to different coordinate time scales with a shifted origin.

Consider two satellites A and B: since the association $t_{A0} = t_A(\tau_{A0})$ and $t_{B0} = t_B(\tau_{B0})$ is arbitrary for both satellites, the coordinate time scales each satellite transforms to are shifted by an amount $t_B - t_A = \delta t_{AB}$, which corresponds to the coordinate time offset between the two satellite clocks. This offset can be determined by comparing the transformed proper timestamps associated with the same event observed by both satellites, e.g. with a time transfer method as presented in the following section.

Thanks to the approximate knowledge of the satellites' position and velocity, the integral on the right side of (2) can be computed, and any proper time scale can be transformed into one instance of coordinate time. An incorrect knowledge of position and velocity of the satellite affects the proper-to-coordinate transformation. As shown in (Dassié & Giorgi, 2021), the error margins are generous: for integrals over 1 s, we are still able to transform the satellite clocks timestamps into coordinate time instants with picosecond-level accuracy even with position errors of the order of thousands of meters and velocity errors in the order of meters per second.

2.3 TWO-WAY TIME TRANSFER

Let us consider a TWTT scheme as presented in Figure 1. Consider an ideal clock located inside satellite A, at position $\boldsymbol{r}_A$, beating proper time τ_A, and a second ideal clock beating proper time τ_B, located at $\boldsymbol{r}_B$. We assume that the two clocks are not coordinate synchronized, and therefore the coordinate time scales they transform their proper timestamps to present a relative offset $t_B - t_A = \delta t_{AB}$ given in coordinate time, which is the quantity to determine with a TWTT. Satellite A transmits a signal towards satellite B with timestamp τ_{A0}, that is measured as received at time τ_{B1}. In the same way a communication in the opposite direction takes place: satellite B transmits a signal with timestamp τ_{B2} that is received at time τ_{A3} at satellite A. The exchange is represented here as sequential, but the mutual transmission could also be nearly synchronous, depending on the degree of prior de-synchronization of the satellite clocks.

Assume that the two satellites use proper instants τ_{A0} and τ_{B0} as lower bound of the integral in (2). These are arbitrarily associated to coordinate time instants $t_{A0} = t_A(\tau_{A0})$ and $t_{B0} = t_B(\tau_{B0})$. With (2), satellite A can determine the coordinate time instants associated to the measured instants of emission $t_{A0} = t_A(\tau_{A0})$ and reception $t_{A3} = t_A(\tau_{A3})$. Analogously, satellite B can transform its measures into coordinate time instants of reception $t_{B1} = t_B(\tau_{B1})$ and emission $t_{B2} = t_B(\tau_{B2})$.

The goal of the TWTT is to determine the inter-satellite clock offset δt_{AB} by comparing the instants associated to the same event given in the different coordinate time scales t_A and t_B. In the specific case of a TWTT, the common events are the instants of reception of the signal at both ends.

We can retrieve the instants of reception in both time scales by exploiting the properties of light propagation and with approximate satellites' positions at the moments of emission t_0 and reception t_1. From the Schwarzschild metric we can also determine the amount of coordinate time that an electromagnetic signal needs to travel between the positions $\boldsymbol{r}_A(t_0)$ and $\boldsymbol{r}_B(t_1)$ of the two satellites (Ashby, 2003):

$$T_{AB} = \frac{||\boldsymbol{r}_B(t_1) - \boldsymbol{r}_A(t_0)||}{c} + \frac{2GM}{c^3} \ln\left(\frac{r_A(t_0) + r_B(t_1) + ||\boldsymbol{r}_B(t_1) - \boldsymbol{r}_A(t_0)||}{r_A(t_0) + r_B(t_1) - ||\boldsymbol{r}_B(t_1) - \boldsymbol{r}_A(t_0)||}\right) \tag{3}$$

where $r = ||\boldsymbol{r}||$. The first term on the right-hand side of (3) is the classical Euclidean travel time from satellite A to satellite B. The second term represents an additional delay resulting from the time dilation experienced by light when travelling through a gravitational field and is a purely relativistic effect. This term is called Shapiro delay (Ashby, 2003).
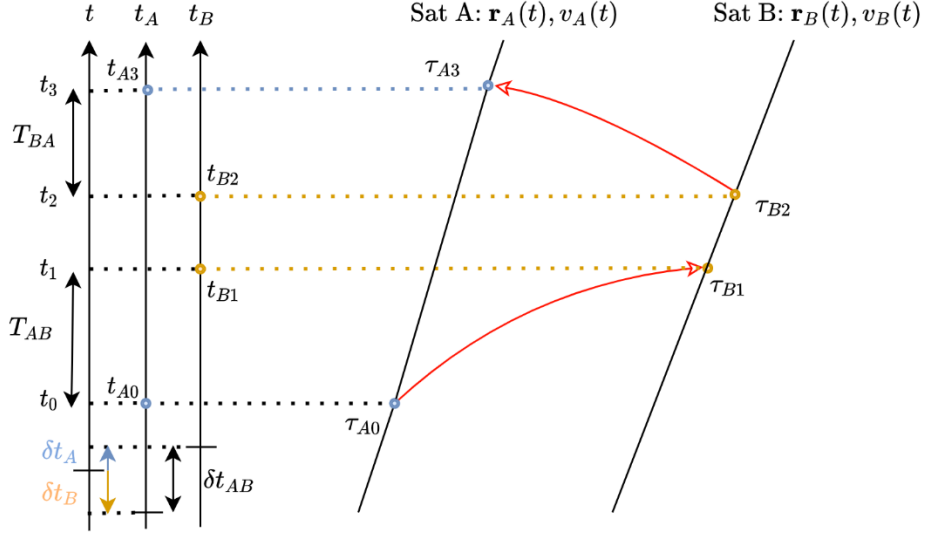
Figure 1. *The trajectories of satellites A and B with the instants of transmission and reception in both ways of the exchange.*

Being able to compute the propagation delays T_{AB} and T_{BA} thanks to the approximate knowledge of the positions of both satellites, the two satellites can estimate the moments of reception at the other end expressed in their own realization of coordinate time scale:

$$\text{Estimated instants of reception:} \quad t_{A1} = t_{A0} + T_{AB}, \quad t_{B3} = t_{B2} + T_{BA} \tag{4}$$

These same instants are also measured by the respective parties and transformed into coordinate time:

$$\text{Reception instants transformed from measurement:} \quad t_{B1} = t_B(\tau_{B1}), \quad t_{A3} = t_A(\tau_{A3}) \tag{5}$$

Therefore, as long as the exchange of signals is performed over a short time span, the timestamps associated to the same instants expressed in the two instances of coordinate time satisfy the following requirements:

$$t_{B1} = t_{A1} + \delta t_{AB}, \quad t_{A3} = t_{B3} - \delta t_{AB} \tag{6}$$

Substituting (4) into (6), subtracting them from each other, and isolating δt_{AB} we obtain:

$$\delta t_{AB} = \frac{1}{2}\left(t_{B1} - (t_{A0} + T_{AB})\right) - \frac{1}{2}\left(t_{A3} - (t_{B2} + T_{BA})\right) \tag{7}$$

The first terms in both brackets of (7) are obtained from measurements at reception at both sides. The second terms in the brackets are the estimated instants of reception computed in the timescale of the emitter with the approximate knowledge of the satellites' positions and trajectories using (3). Reordering the term in (7) one can see that the propagation times appear in the form of difference $\frac{1}{2}(T_{BA} - T_{AB})$, so one can use a simplified version of (3) where only the Euclidean term is considered for both T_{AB} and T_{BA}. The difference of Shapiro delays in the roundtrip is much lower than a picosecond and can be neglected (Dassié & Giorgi, 2021).

An error in the determination of the position of a satellite would impact the estimation of the difference in the roundtrip propagation time and consequently result in a biased estimate of the inter-satellite clock offset. By keeping the round-trip exchange as symmetric as possible, the quantity $\frac{1}{2}(T_{BA} - T_{AB})$ in (7) becomes very small and the impact of biases is also mitigated. Maximal symmetry can be achieved by intentionally having an almost simultaneous emission of signals at both ends.

In the appendix we demonstrate that, with an almost symmetrical exchange, as long as orbital errors are approximately constants or their dynamic is relatively slow (millimeter per second), a meter-level orbit accuracy is enough to keep their impact on the last term below the picosecond. Both conditions are assumed to be satisfied within the current capabilities of POD in GNSSs.

2.3 SYSTEM INITIALIZATION AND OPERATION

Consider N non-synchronized satellites with free-running clocks generating proper time τ_i. Let each couple of satellites perform a coarse TWTT via the following simplified expression:

$$\delta\tau_{AB} = \frac{1}{2}(\tau_{B1} - \tau_{A0}) - \frac{1}{2}(\tau_{A3} - \tau_{B2}) \tag{8}$$

This is a rough first approximation of the inter-satellite clock offset δt_{AB} in coordinate time. As shown in the Appendix, the determination of this approximate offset would guarantee a synchronization of all satellites within a few microseconds. According to a pre-determined schedule that considers link duration and visibility constraints, the satellites perform a high accuracy TWTT in a loop topology (Deprez & Giorgi, 2021; Giorgi et al., 2019). Since all satellites have performed a prior coarse synchronization and have an approximate knowledge of their relative positions, they can choose the timestamps within a series of exchanges that lead to the minimum amount of asymmetry in the communication. Knowing their approximate position and velocity, the satellites can transform their proper timestamps into coordinate timestamps with (2). Using (7), each connected couple of satellites is able to retrieve the relative clock offset while keeping the impact of position errors below the picosecond threshold thanks to the symmetric exchange. The results of these TWTTs are a set of N relative clock offsets δt_{AB} given in coordinate time and determined with picosecond accuracy. Once the satellites are synchronized to picosecond-level, the signal exchanges allow one-way ranging with (sub-)millimeter precision. The inter-satellite ranges are used to enhance POD products, thus reducing the error on the estimated position and velocity of the satellites, which in turn improves the proper-to-coordinate time transformation and further reduces the inaccuracies in the determination of the last term of (7).

From each TWTT between satellites A and B we obtain the following quantity:

$$z_{AB}(t) = \delta t_{AB}(t) + v_{AB}(t) + \Delta(t) = x_B(t) - x_A(t) + v_{AB}(t) + \Delta(t) \tag{9}$$

where $x_A(t)$, $x_B(t)$ are the actual phases of the two clocks at time instant t, $v_{AB} \sim \mathcal{N}(0, R)$ is the measurement noise with variance R due to the tracking loops enabling the generation of timestamps, and $\Delta(t)$ is a bias arising from modelling inaccuracies of the TWTT. These could be due to inaccurate modelling of hardware delays, inaccuracies in position and velocity of the satellites, and other modeling or calibration errors. The observation model (9) is at the basis of the system synchronization algorithm presented in the next section.

3. SPACE-BASED DISTRIBUTED CLOCK ENSEMBLE

Thanks to the OISLs, the pairwise time differences between satellites are distributed across the constellation with a very small delay. Thus, having these measurements available, each satellite can run the ensembling algorithm and generate a local copy of the system time. The KST is defined as the Implicit Ensemble Mean (IEM) $\overline{x_0}$ of the ensemble formed by all the oscillators onboard the satellites (Brown, 1990). The algorithm requires the knowledge of the time state of each clock participating in the ensemble. However, these cannot be directly observed, since the available measurements are pairwise time differences between satellite couples, as modeled in (9). Thus, the time state must be estimated given the available observations. This is done with a Kalman filter, which is based on a clock dynamic model and measurement model.

The states used to describe the clocks depend on the choice of clock model: in this work we employ a two-states clock model with constant frequency drift and additional Gauss-Markov processes (Greenhall, 2006; Trainotti, 2019). Each clock i is modelled using a state $x_i(t)$ for the phase difference to an ideal clock and $y_i(t)$ for the fraction frequency difference to an ideal clock. One or more Gauss-Markov processes can be added to the model to improve the description of the clock behavior: in this case the state vector is extended to accommodate the additional states. Without loss of generality, in the following equations we do not add any states for Gauss-Markov processes. The modifications to the model matrices can be seen in (Greenhall, 2006). The state vector of the entire ensemble x is formed by stacking the states of the M clocks:

$$\boldsymbol{x}(t)^\top = \begin{pmatrix} x_A(t) & y_A(t) & x_B(t) & y_B(t) & \cdots & x_M(t) & y_M(t) \end{pmatrix} \qquad (10)$$

The discrete-time dynamic equation describes the behavior of the free running clocks:

$$\boldsymbol{x}(t + \Delta t) = \boldsymbol{\Phi}(\Delta t)\boldsymbol{x}(t) + \boldsymbol{D}(\Delta t) + \boldsymbol{w}(t) \qquad (11)$$

where Δt is the constant time discretization, $\boldsymbol{\Phi}$ is the state propagation matrix, $\boldsymbol{D}$ is the constant frequency drift, and $\boldsymbol{w} \sim \mathcal{N}(0, \boldsymbol{Q}(\Delta t))$ is the clocks process noise, with associated covariance matrix $\boldsymbol{Q}$. The matrices $\boldsymbol{\Phi}$ and $\boldsymbol{Q}$ are block diagonal, each block corresponding to the matrices of the single clock i, and the drift vector $\boldsymbol{D}$ is formed by stacking the vectors of the single clocks, where d_i is the constant frequency drift of clock i:

$$\boldsymbol{\Phi}_{ii}(\Delta t) = \begin{pmatrix} 1 & \Delta t \\ 0 & 1 \end{pmatrix} \qquad \boldsymbol{Q}_{ii}(\Delta t) = \begin{pmatrix} q_i^I \Delta t + q_i^{II} \dfrac{\Delta t^3}{3} & q_i^{II} \dfrac{\Delta t^2}{2} \\ q_i^{II} \dfrac{\Delta t^2}{2} & q_i^{II} \Delta t \end{pmatrix} \qquad \boldsymbol{D}_i(\Delta t) = \begin{pmatrix} \dfrac{\Delta t^2}{2} \\ \Delta t \end{pmatrix} d_i \qquad (12)$$

The parameters q_i^I and q_i^{II} describe the intensity of the process noise acting on the phase and frequency of each clock. They can be determined by characterizing the clock's behavior, for instance by fitting the measured overlapping Allan deviation (OADEV) (Trainotti et al., 2019).

The ensemble model is completed by adding a measurement equation, linking the observed differences between satellites to their states, as in (9):

$$\boldsymbol{z}(t) = \boldsymbol{Hx}(t) + \boldsymbol{v}(t) \qquad (13)$$

where $\boldsymbol{z}$ is the vector of observations, and $\mathbf{H}$ the measurement matrix. The measurement matrix selects the readings of the clocks involved in every single comparison, thus it depends on the topology of the measurement system (i.e. how the satellites are connected to each other). In nominal conditions and with a perfect model, the measurement noise distributes as $\boldsymbol{v} \sim \mathcal{N}(0, \boldsymbol{R})$, with associated covariance matrix $\boldsymbol{R}$. In the following we will consider also non-nominal cases with measurement biases.

The available measurements only include differences between clocks readings and thus an observer has no direct access to the states of a single clock $\boldsymbol{x}_i$., A Kalman filter is used to estimate the clocks' states given the available observations and provide the state estimate $\widehat{\boldsymbol{x}}$. However, the state unobservability causes the covariance associated to the state estimate to grow unbounded (Greenhall, 2006). This can be mitigated using a covariance reduction method. The Kalman filter estimates the states of the ensemble in an iterative way by first predicting the state in the next step using the clock model, and then corrects the prediction using the available measurements:

Prediction
$$\widehat{\boldsymbol{x}}^-(t) = \boldsymbol{\Phi}\widehat{\boldsymbol{x}}(t - \Delta t) + \boldsymbol{D}$$
$$\boldsymbol{P}^-(t) = \boldsymbol{\Phi}\boldsymbol{P}(t - \Delta t)\boldsymbol{\Phi}^\top + \boldsymbol{Q}$$

Update
$$\boldsymbol{K}(t) = \boldsymbol{P}^-(t)\boldsymbol{H}^\top[\boldsymbol{H}\boldsymbol{P}^-(t)\boldsymbol{H}^\top + \boldsymbol{R}]^{-1}$$
$$\widehat{\boldsymbol{x}}(t) = \widehat{\boldsymbol{x}}^-(t) + \boldsymbol{K}(t)[\boldsymbol{z}(t) - \boldsymbol{H}\widehat{\boldsymbol{x}}^-(t)]$$
$$\widetilde{\boldsymbol{P}}(t) = [\boldsymbol{I} - \boldsymbol{K}(t)\boldsymbol{H}]\boldsymbol{P}^-(t)$$

Covariance reduction
$$\boldsymbol{P}(t) = \widetilde{\boldsymbol{P}}(t) - \overline{\boldsymbol{H}}\left[\overline{\boldsymbol{H}}^\top \widetilde{\boldsymbol{P}}(t)^{-1}\overline{\boldsymbol{H}}\right]^{-1}\overline{\boldsymbol{H}}^\top$$

where $\widehat{\boldsymbol{x}}^-$ is the predicted estimate with associated error covariance $\boldsymbol{P}^-$, $\boldsymbol{K}$ is the Kalman gain, $\widehat{\boldsymbol{x}}$ is the updated estimated with associated error covariance $\widetilde{\boldsymbol{P}}$, and is the $\boldsymbol{I}$ identity matrix. The reduced error covariance $\boldsymbol{P}$ is computed by using the matrix $\overline{\boldsymbol{H}}$, obtained by vertically stacking N 2x2 identity matrices, where N is the number of clocks in the ensemble. If Gauss-Markov processes are used in the clock model, the matrix $\widetilde{\boldsymbol{P}}$ must be modified by removing the rows and columns which correspond to the states describing the additional processes.

With the estimates of the clock states $\widehat{\boldsymbol{x}}$, it is possible to define the IEM:

$$\overline{x_0} = \boldsymbol{a}^\top(\boldsymbol{x} - \widehat{\boldsymbol{x}}) \qquad (14)$$

where $\boldsymbol{a}$ is a vector of weights. The IEM is therefore a weighted average of the state vector estimation error. There exist different methods to compute the weights $\boldsymbol{a}$, here we use the approach shown in (Davis, 2005). The IEM is the best estimate of the ideal time given the available clocks and their measurements, and it is used as definition of KST. However, it is unobservable, since the clock states $\boldsymbol{x}$ are not accessible. To obtain a physical realization of the IEM, a control loop is applied to a local oscillator following the scheme presented in (Schmidt et al, 2018; Trainotti, Schmidt & Furthner, 2019). It consists of a second Kalman filter which estimates the deviation of the steered clock $\hat{\boldsymbol{x}}_S(t)$ from the ideal clock, and a controller. The controller computes the steering action $u(t) = -\boldsymbol{G}\hat{\boldsymbol{x}}_S(t)$ to be applied to the steered clock. Different methods can be used to design the steering gain $\boldsymbol{G}$, in this work we use the pole placement (PP) technique (Schmidt, Trainotti & Furthner, 2018). The gain matrix is computed based on the design parameter $\lambda \in [0,1]$:

$$G = \left[\frac{(1-\lambda)^2}{\Delta t_S} \quad 1-\lambda^2 \right] \tag{15}$$

where Δt_S is the steering rate, namely how often the local controller is steered. For this work we use $\lambda = 0.2$ and $\Delta t_S = 1\ s$.

In the framework of Kepler, each satellite receives the differential measurements $\boldsymbol{z}$, and runs a Kalman filter to obtain the state estimate of all the constellation's clocks. It then steers an onboard oscillator to realize a local copy of the IEM, corresponding to KST. Given noisy and biased measurements and different local steered oscillators, each satellite generates a slightly different time scale. It is then natural to ask how well the local realization represents KST, and how much the onboard realizations differ from one another. Furthermore, we want to understand what happens when residual biases are present in the observed differences among satellites, which can arise due to various effect, as mentioned in section 2.

3.1 SIMULATION SCENARIOS

We simulate the system time generation in different scenarios, to understand how different design choices influence the achievable synchronization level. The cases are summarized in Table 1.

Table 1We analyzed two system architectures, hereafter named "Kepler fast track" (Günther, 2022) and "full Kepler" (Günther, 2018, Giorgi et al, 2019;). The former is a simplified approach of the full Kepler concept: with the goal of speeding up the development and deployment of a Kepler architecture, critical components (e.g. optical iodine frequency references, cavity-stabilized lasers) are traded with components with higher technology readiness levels (TRL), such as ultra-stable oscillators (USOs). Additionally, in the Kepler fast track architecture the LEO segment is only used as a space-based monitoring and calibration layer, without establishing optical links to the MEO segment, and it does not contribute to the system synchronization: only the MEO clocks form an ensemble exploiting the capabilities of OISLs (scenarios 1 and 2).
Conversely, in the full Kepler architecture, each LEO satellite is assumed equipped with an USO and an optical iodine clock, and it can optically link to the MEO segment. The two-way LEO-MEO link allows the inclusion of all LEO clocks in the ensemble (scenarios 3 and 4).
For all scenarios we consider the nominal case in which the differential clock measurements are only affected by zero-mean Gaussian noise, with standard deviation of either 0.3 ps or 3 ps. The lower noise level corresponds to the achievable link precision demonstrated experimentally (Surof et al., 2019; Calvo et al., 2020, Surof et al., 2022), while higher noise level considers possible unmodelled effects. In the two full Kepler scenarios, we assume that the measurements between clocks onboard the same LEO satellite are affected by noise with standard deviation of 1fs.

Table 1: List of scenarios simulated for the time scale generation

	Scenario	Clock(s) on 24 MEO satellites	MEO-MEO measurement noise level	Clock(s) on 6 LEO satellites	MEO-LEO measurement noise level
1	Kepler fast track	USO	0.3 ps (0.1 mm)	None	No connection
2	Kepler fast track	USO	3.0 ps (1.0 mm)	None	No connection
3	Full Kepler	USO	0.3 ps (0.1 mm)	USO+iodine clock	0.3 ps (0.1 mm)
4	Full Kepler	USO	3.0 ps (1.0 mm)	USO+iodine clock	3.0 ps (1.0 mm)

3.2 TRANSIENT PHASE AND STEADY-STATE

To verify the convergence of the steered clocks to the IEM, we analyze the initialization phase in the scenario 1. The clock phase is initialized to a random value in the interval 0.5 ± 1 ns, since at the initial step the clocks are free-running and yet to be synchronized. The definition of the center of the interval is arbitrary, but the range is representative of current system synchronization capabilities in GNSSs. Figure 2 shows the transient segment of the steering process of the third scenario: from the initial value, the steered clocks gradually converge to the system IEM. Within the initial 50 s, the clocks follow the IEM within a range of about ± 10 ps. As seen in Figure 3, at steady-state the steered clocks reach the IEM and follow it within a band of few picoseconds.
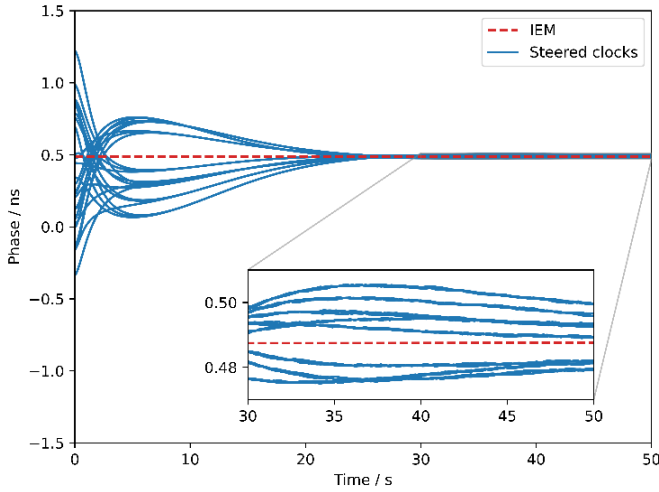
Figure 2: Transient phase of the steered clocks. The steered oscillators converge to the IEM.
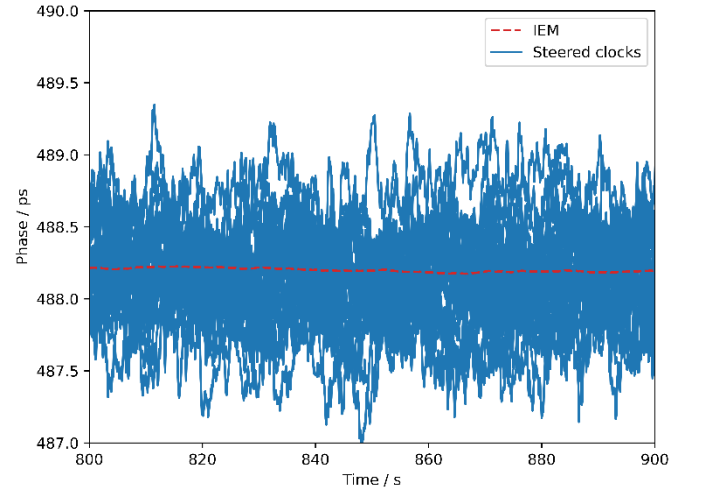
Figure 3: Steady-state steering of the clock around the IEM.

3.3 STEADY-STATE SYNCHRONIZATION ERROR

In order to compare the performance of the clock steering system in different scenarios, we introduce the concept of steady-state synchronization error. We define two errors, namely the difference of each realization to the IEM $\delta_{IEM,i}(t)$, and the maximum difference between any two realizations $\delta_{max}(t)$:

$$\delta_{IEM,i}(t) = x_{S,i}(t) - \overline{x_0}(t) \tag{16}$$

$$\delta_{max}(t) = max_{ij}\left(\left|x_{S,i}(t) - x_{S,j}(t)\right|\right) = max_i\left(x_{S,i}(t)\right) - min_i\left(x_{S,i}(t)\right) \forall i \neq j \tag{17}$$

where $x_{S,i}(t)$ is the phase of the steered clock i at time t.

Figure 4 shows the statistics of $\delta_{IEM,i}(t)$ for the steady-state of scenario 3 (after the 50 s initialization period). The differences distribute according to a zero-mean Gaussian distribution. The right plot shows the cumulative distribution of the absolute values, as well as the mean distribution across the realizations. From the plot we can see that 95% of the time the steered clocks are within ± 0.57 ps from the IEM. The distribution of the maximum difference between steered clocks is shown in Figure 5: 95% of the time any two clocks are synchronized within 1.54 ps from each other.
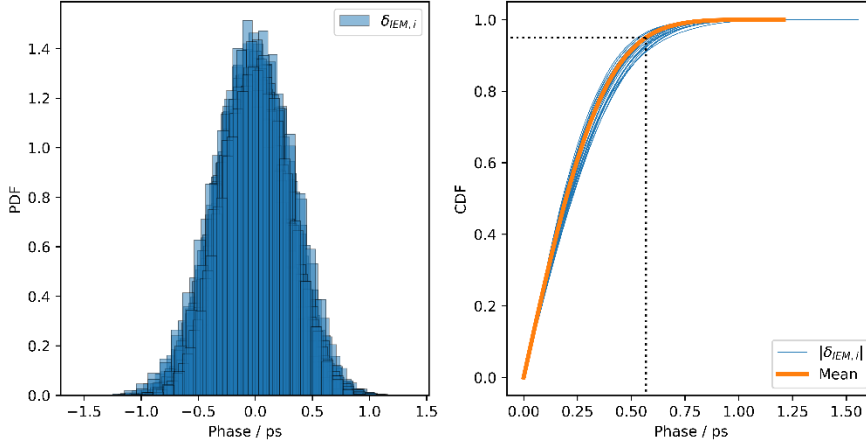
Figure 4: Statistics of the differences between steered clocks and IEM in the steady-state phase of scenario 3
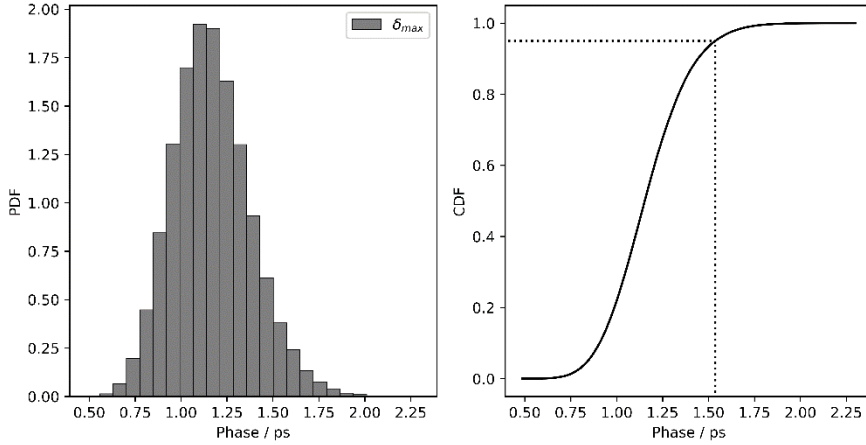
Figure 5: Statistics of the maximum difference between steered clocks in the steady-state of scenario 3

In the framework of Kepler, the most important measure of synchronization is the difference among clocks, $\delta_{max}(t)$, whereas the desynchronization with respect to the IEM is of secondary importance: from the user perspective, it does not matter if the clocks diverge from the ensemble mean, as long as they are close to each other and emit signals simultaneously. The IEM is an unobservable reference characterizing the timing system, but it is fully transparent to the user. For this reason, in the following analyses we are only going to compare the scenarios in terms of maximum desynchronization among satellites $\delta_{max}(t)$.

3.4 COMPARISON OF DIFFERENT SCENARIO – NOMINAL CASE

To compare the performance of the different constellation scenarios listed in Table 1, we plot in Figure 6 the CDF of the synchronization error among clocks, δ_{max}. The green lines are for the Kepler fast track scenarios (1 and 2), and red is used of the full Kepler scenarios (3 and 4). The downward triangle marker indicates the scenarios with low measurement noise (1 and 3), while the upward triangle marks the high measurement noise (2 and 4).
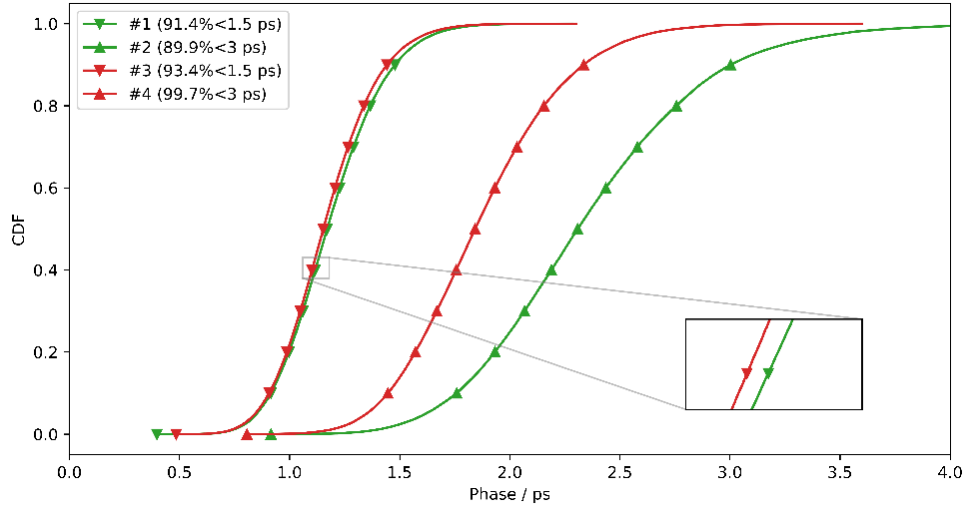
Figure 6: Synchronization error among clocks in the four scenarios of Table 1, for a nominal case without biases. The percentages in brackets give the probability for which a value is below the given level.

In the case of lower measurement noise, the two scenarios show similar performance, with synchronization errors below 1.5 ps for more than 90% of the time. If the measurement noise covariance is increased, the distribution of the synchronization error moves to higher values and has longer tails. Full Kepler appears to be less sensitive to an increase of measurement noise, while Kepler fast track is more affected, with errors below 3 ps for about 90% of the time. The better performance of full Kepler is due to the presence of the local USO-iodine measurements onboard the LEO satellites, which present very low measurement noise.

3.5 INJECTION OF BIAS

To assess the impact of observation biases, we simulate additional six scenarios by including an unmodelled bias in the pairwise time transfer between satellites. We modify (13) as:

$$z(t) = Hx(t) + v(t) + \Delta(t) \tag{18}$$

where $\Delta(t)$ is the magnitude of the injected bias. In a first set of simulations, we introduce a time-constant bias with three levels of magnitude:

$$\Delta(t) = \mu b \tag{19}$$

where μ is a vector of random values uniformly distributed between 0 and 1 and b is the bias magnitude. In this work we consider three bias magnitudes, namely 1 ps, 3 ps and 5 ps. In the full Kepler scenarios, the measurements onboard the LEO satellites are not affected by these biases. The resulting synchronization errors $\delta_{max}(t)$ are shown in Figure 7. The green lines represent the case of Kepler fast track (scenarios 1 and 2), while the red ones are for full Kepler (scenarios 3 and 4). The left plots are for the case with reduced measurement noise, the right ones for the higher level. The fading color indicates the increasing level of bias. The injected measurement biases show a direct influence to the synchronization error. The effect in Kepler fast track is almost one to one, meaning that a bias of 3 ps increases the maximum synchronization error of about 3 ps. The increase is reduced in the case of full Kepler, due to the presence of the bias-free measurements between iodine frequency references and USOs on the LEO satellites.
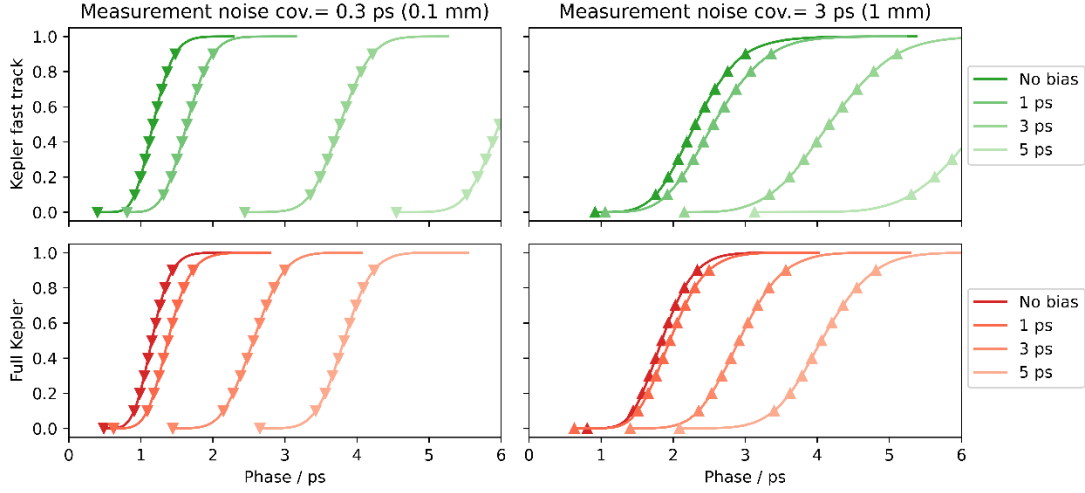
Figure 7: Synchronization error among clocks in the presence of a constant measurement bias. The green lines represent the case of Kepler fast track (scenarios 1 and 2), while the red ones are for full Kepler (scenarios 3 and 4). Lighter shades of color are used for increasing measurement bias.

3.6 CLOSED AND OPEN RING TOPOLOGY

The scenarios in Table 1 all consider a closed ring topology, meaning that the measurement ring of the MEO satellites is closed, providing measurements 2-1, 3-2, 4-3, ... , 24-23, 1-24. We performed an additional analysis by removing the last measurement, and thus leaving the ring open, to check whether the constellation is more or less affected by measurement biases. The synchronization error is shown in Figure 8 for the scenarios 1 and 3, in closed or open ring configuration, with or without a 5 ps constant measurement bias. The dotted-dashed lines refer to the open ring cases. Without measurement biases, the open ring scenarios show a slightly worse performance of synchronization, but still below 2 ps. However, the open ring configuration is sensitive to measurement biases, as inferred from the right plots. The biases are seriously impacting the synchronization system, with error reaching values of about 17 ps for full Kepler and 57 ps for Kepler fast track. When the ring is closed, the additional measurement adds a constraint to the system, namely that the sum of the clock differences along the ring must be zero (without biases and noise):

$$\delta t_{N1} + \sum_{i=1}^{N-1} \delta t_{i,i+1} = 0 \qquad (20)$$

Thanks to the constraint, the system can partially filter the measurement biases out and provide a better estimation of the clocks' states. When the additional link is missing, the system is no longer fully constrained, and biases have a larger impact on the synchronization concept. In the case of full Kepler, the additional LEO-MEO measurements improve the geometry of the timing system, and the impact of biases is largely mitigated even in the case of an open ring configuration.
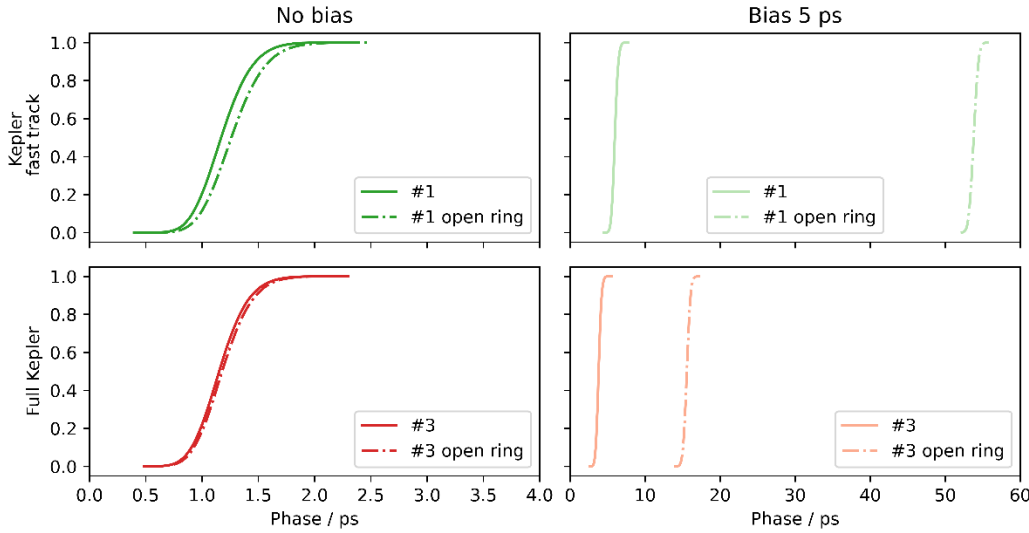
Figure 8: Synchronization error with (right) and without (left) a 5 ps measurement bias, in an open ring and closed ring constellation topology.

4. CONCLUSION

In this paper we use TWTTs between pairs of satellites to synchronize a constellation of N satellites equipped with clocks of various type, without prior synchronization. System synchronization can be achieved from a "cold-start" in two consecutive steps: a first step is required to perform an initial non-relativistic coarse synchronization to align all satellite clocks (in a coordinate time scale) within a few microseconds. Then, at predetermined intervals, all satellites perform pairwise relativistic time transfer. The coarse synchronization step mitigates the error induced by satellite position and velocity uncertainties in the estimation of the round-trip propagation delay. With a nearly-symmetric two-way exchange of signals, the Euclidean expression for the propagation of light is sufficient to achieve picosecond synchronization, provided meter-level orbit determination of both satellites is available, and the orbit error dynamics is negligible of the TWTT exchange (<1 s). The result of these exchanges are relative offsets in coordinate time that are distributed via OISLs across the whole constellation and are used as input for the proposed system time generation algorithm. The ensembling algorithm is based on a Kalman filter, which estimates the clocks' states given an underlying system model and the observed clock offsets. Finally, the steering control signal produced on each satellite with a second Kalman filter is applied to the local reference oscillator, thus realizing the system-wide synchronization. In the initialization phase, the steered clocks quickly converge from their initial status to the IEM, and the steering system forces them to follow the IEM in the long term.

In this paper we analyzed how the measurement noise and biases are expected to impact the constellation synchronization performance.

We analyzed the steady-state synchronization error, i.e. the maximum recorded difference between the clocks on any two satellites of the constellation. Both the "Kepler fast track" and "full Kepler" architectures achieve similar synchronization levels (1.5 ps about 95% of the times) under nominal conditions. An increase in the measurement noise covariance to 3 ps brings the synchronization error to circa 3 ps.

To simulate unmodelled systematic effects, we introduced constant measurement biases in the system, and analyzed the resulting synchronization. The synchronization level is directly influenced by the biases, with the full Kepler scenario showing better performance than Kepler fast track. This is due to the presence of the optical iodine references on the LEO satellites and the onboard measurements.

Finally, an open ring measurement topology was compared to a closed ring. The closure of the measurement ring introduces a constraint in the timing system, which can better filter measurement biases. Furthermore, the additional LEO-MEO links allows full Kepler to better deal with unmodelled biases even in the open ring configuration.

In future work we plan to formally derive the transfer function of the (controlled) system, so that it is possible to analyze how the steering loop reacts to (or compensate for) unmodelled noises and biases. Further, a sensitivity analysis on the steering parameters can be carried out.

A space-based system time scale is completely autonomously determined by the orbiting satellites; there is in principle no need for a ground infrastructure to support the synchronization process. The role of the ground segment is only necessary when establishing a connection to terrestrial time scales, as for example UTC. The space-to-ground link can be established either with an a-posteriori estimate of the offset between the "space clock" and the reference Earth time scale based on broadcast signals, or with one or more optical links between a satellite of the Kepler constellation and one of the ground stations.

REFERENCES

Ashby, N. (2003). Relativity in the Global Positioning System. Living Reviews in Relativity, 6(1), 1. doi:10.12942/lrr-2003-1

Brown, K. R. (1991). The Theory of the GPS Composite Clock. Proceedings of the 4th International Technical Meeting of the Satellite Division of The Institute of Navigation (ION GPS) (pp. 223–242). ION.

Calvo, R. M., Poliak, J., Surof, J., & Wolf, R. (2020). Evaluation of optical ranging and frequency transfer for the Kepler system: preliminary laboratory tests. 2020 European Navigation Conference (ENC). IEEE. doi:10.23919/enc48637.2020.9317374

Dassié, M., & Giorgi, G. (2021). Relativistic Modelling for Accurate Time Transfer via Optical Inter-Satellite Links. Aerotecnica Missili & Spazio. doi:10.1007/s42496-021-00087-1

Davis, J. A., Greenhall, C. A., & Stacey, P. W. (2005). A Kalman Filter Clock Algorithm for Use in the Presence of Flicker Frequency Modulation Noise. Metrologia, 42(1) (pp. 1-10)

Deprez, C., & Giorgi, G. (2021). Operational Envelope and Link Scheduling for Inter-satellite Links in Next-generation GNSSs. Proceedings of the IEEE Aerospace Conference 2021, Big Sky, MT, USA. doi: 10.1109/AERO50100.2021.9438393

Greenhall, C. A. (2006). A Kalman Filter Clock Ensemble Algorithm that Admits Measurement Noise. Metrologia, 43(4), S311–S321. doi:10.1088/0026-1394/43/4/S19

Giorgi, G., Kroese, B., & Michalak, G. (2019). Future GNSS constellations with optical inter-satellite links. Preliminary space segment analyses. Proceedings of the IEEE Aerospace Conference 2019, Big Sky, MT, USA. doi: 10.1109/AERO.2019.8742105

Giorgi, G., Schmidt, T.D., Trainotti, C., Mata-Calvo, R., Fuchs, C., Hoque, M.M., Berdermann, J., Furthner, J., Günther, C., Schuldt, T., Sanjuan, J., Gohlke, M., Oswald, M., Braxmaier, C., Balidakis, K., Dick, G., Flechtner, F., Ge, M., Glaser, S., König, R., Michalak, G., Murböck, M., Semmling, M., & Schuh, H. (2019). Advanced Technologies for Satellite Navigation and Geodesy. Advances in Space Research, 64(6) (pp. 1256-1273). doi: 10.1016/j.asr.2019.06.01

Günther, C. (2018). Kepler - Satellite Navigation without Clocks and Ground Infrastructure. Proceedings of the 31st International Technical Meeting of the Satellite Division of the Institute of Navigation 2018 (ION GNSS+ 2018) (pp. 849–856). doi:10.33012/2018.15997

Günther, C., Michalak, G., Trainotti, C., Giorgi, G. & Neumayer, K.-H. (2022). Kepler Fast Track. Proceedings of the 10th Workshop on Satellite Navigation Technologies (NAVITEC 2022), European Space Research and Technology Centre (ESTEC), Noordwijk, The Netherlands.

Klioner, S. A. (1992). The problem of clock synchronization: A relativistic approach. Celestial Mechanics and Dynamical Astronomy, 53(1), 81–109. doi:10.1007/bf00049363

Michalak, G., Dassie, M., Testa, A., Giorgi, G., Günther, C., & Neumayer, K.H. (2022). Signal-in-Space Range Error Analysis of the Simulated Broadcast Ephemerides for the Kepler System. ION-GNSS+ 2022, to be published

Michalak, G., Glaser, S., Neumayer, K. H., & König, R. (2021). Precise orbit and Earth parameter determination supported by LEO satellites, inter-satellite links and synchronized clocks of a future GNSS. Advances in Space Research, 68(12), 4753–4782. doi:10.1016/j.asr.2021.03.008

Petit, G., & Wolf, P. (2005). Relativistic Theory for Time Comparisons: a Review. Metrologia, 42, S138–S144. doi:10.1088/0026-1394/42/3/S14

Poliak, J., Calvo, R. M., Surof, J., Richerzhagen, M., & Wolf, R. (2018). Laboratory Demonstrator of Optical Inter-satellite Links for the Kepler System. Proceedings of the 31st International Technical Meeting of The Satellite Division of the Institute of Navigation (ION GNSSmathplus 2018) (pp. 861–867). Institute of Navigation. doi:10.33012/2018.15886

Schmidt, T., Trainotti, C., Isoard, J., Giorgi, G., Furthner, J., & Günther, C. (2018). Composite Clock Algorithms for System Time in Global Navigation Satellite Systems. Proceedings of the 31st International Technical Meeting of the Satellite Division of the Institute of Navigation 2018 (ION GNSS+ 2018) (pp. 963–967). doi:10.33012/2018.15891

Schmidt, T., Trainotti, C., Furthner, J. (2019). Comparing Clock Steering Technique Performances in Simulations and Measurements. Proceedings of the 50th Annual Precise Time and Time Interval Systems and Applications Meeting. doi: 10.33012/2019.16758

Schutz, B. (2009). A First Course in General Relativity. Cambridge University Press; 2nd Ed. (2009).

Surof, J., Poliak, J., Calvo, R. M., Richerzhagen, M., Wolf, R., & Schmidt, T. (2019). Laboratory Characterization of Optical Inter-satellite Links for Future GNSS. Proceedings of the 32nd International Technical Meeting of the Satellite Division of The Institute of Navigation (ION GNSSmathplus 2019) (pp. 1051–1058). Institute of Navigation. doi:10.33012/2019.17042

Surof, J., Poliak, J., Wolf, R., Macri, L., Calvo, R. M., Blümel, L., Dominguez, P., et al. (2022). Validation of Kepler Time and Frequency Transfer on a Terrestrial range of 10.45km. ION GNSS+ 2022, to be published.

Trainotti, C., Schmidt, T. D., & Furthner, J. (2019). Simulating the Realization of a Mixed Clock Ensemble. 2019 Joint Conference of the IEEE International Frequency Control Symposium and European Frequency and Time Forum (EFTF/IFC). IEEE. doi:10.1109/fcs.2019.8856103

Trainotti, C., Schmidt, T.D., & Furthner, J. (2019). Comparison of Clock Models in View of Clock Composition, Clock Steering and Measurement Fitting. Proceedings of the ION Precise Time and Time Interval Meeting (PTTI), (pp. 265-283), Reston, VA, USA. doi: 10.33012/2019.16756

Wolf, P. & Petit, G. (1995). Relativistic theory for clock syntonization and the realization of geocentric coordinate times. Astron. Astrophys. 304, (pp. 653–661).

APPENDIX

IMPACT OF POSITION ERRORS ON THE ROUNDTRIP PROPAGATION DELAY DIFFERENCE ESTIMATION

Consider an erroneous knowledge of the position of the satellites where $r_{A,B}(t)$ is the actual position and $r_{A,B}(t) + \delta r_{A,B}(t)$ is the assumed position. Consider the error to be time dependent and growing in a linear way in the neighborhood of any arbitrary instant t_0:

$$\delta r_A(t) \approx \delta r_A(t_0) + \delta \dot{r}_A(t_0)(t - t_0) \tag{21}$$

Such type of position error would impact the determination of the last term of (7):

$$\frac{1}{2}(T_{AB} - T_{BA})_{err} \approx \frac{||r_B(t_1) + \delta r_B(t_1) - r_A(t_0) - \delta r_A(t_0)||}{2c} - \frac{||r_A(t_3) + \delta r_A(t_3) - r_B(t_2) - \delta r_B(t_2)||}{2c} \tag{22}$$

Expanding (22) and representing the time-dependent errors as in (21) we obtain:

$$
\begin{aligned}
\frac{1}{2}(T_{AB} &- T_{BA})_{err} - \frac{1}{2}(T_{AB} - T_{BA}) \\
&\approx \frac{(N_{AB} + N_{BA})^T (\delta r_B(t_0) - \delta r_A(t_0))}{2c} + \frac{N_{AB}^T \delta \dot{r}_B(t_0) T_{AB}}{2c} \\
&- \frac{N_{BA}^T [\delta \dot{r}_A(t_0)(T_{AB} + (t_2 - t_1) + T_{BA}) - \delta \dot{r}_B(t_0)(T_{AB} + (t_2 - t_1))]}{2c}
\end{aligned}
\tag{23}
$$

Where N_{AB} and N_{BA} are the line-of-sight vectors in the two directions.
Assume the worst-case scenario where $\delta r_0 = \delta r_B(t_0) = -\delta r_A(t_0)$ and $\delta \dot{r}_0 = \delta \dot{r}_B(t_0) = -\delta \dot{r}_A(t_0)$:

$$\frac{1}{2}(T_{AB} - T_{BA})_{err} - \frac{1}{2}(T_{AB} - T_{BA})$$
$$\approx \frac{(N_{AB} + N_{BA})^T \delta r_0}{c} + \frac{N_{AB}^T \delta \dot{r}_0 T_{AB}}{2c} + \frac{N_{BA}^T \delta \dot{r}_0 (2T_{AB} + 2(t_2 - t_1) + T_{BA})}{2c} \tag{24}$$

The first term of (24) is an offset due to a constant error present at the instant of the first transmission. It was shown in (Dassié & Giorgi, 2021) that meter-level position errors still allow this term to remain in the sub-picosecond level. The remaining terms in (24) are offsets arising from the growth of the error during the exchange.

Thanks to the prior coarse synchronization we can choose the instants of emission t_0 and t_2 such that the communication is almost symmetric. Then we would have $N_{AB} \approx -N_{BA}$ and $T_{AB} \approx T_{BA}$:

$$\frac{1}{2}(T_{AB} - T_{BA})_{err} - \frac{1}{2}(T_{AB} - T_{BA}) \approx -\frac{N_{AB}^T \delta \dot{r}_0 \left(T_{AB} + (t_2 - t_1)\right)}{c} \tag{25}$$

The propagation times are of the order of 0.1 s and the re-transmission interval $(t_2 - t_1)$ is usually negative and in the interval $[0, -T_{AB}]$ to make the exchange symmetric. Assuming it to be zero we can see that the position error should not grow more than a few millimeters per second in order to maintain a picosecond accuracy in the determination of the roundtrip propagation delay. Current POD models can determine and predict orbits with better accuracy than that.

COARSE SYNCHRONIZATION ACCURACY

Consider two Kepler MEO satellites A and B orbiting in the same direction on a perfectly circular orbit. Assume that the clocks on the satellites are not rate-corrected, so that $\tau_{A,B} - t_{A,B} = \delta t_{rel,AB}$, where this quantity represents an offset between the proper time readings and the respective readings transformed into a coordinate time t.

The error in the estimation of δt_{AB} using the coarse synchronization shown in (8) is:

$$\delta \tau_{AB} - \delta t_{AB} = \frac{1}{2}(T_{AB} - T_{BA}) + \delta t_{rel,AB} \tag{26}$$

Assume satellite B is in front of satellite A in the direction of motion. In a classical Walker 24/3/1 constellation with perfectly circular orbits and semi-major axis $a = 29601$ km, the satellites on each plane are separated by an angle $\theta = 45°$. The time of travel can be obtained via:

$$T_{AB} = \frac{2a}{c}\sin\left(\frac{\theta}{2} + \frac{\omega}{2}T_{AB}\right), \qquad T_{BA} = \frac{2a}{c}\sin\left(\frac{\theta}{2} - \frac{\omega}{2}T_{BA}\right), \qquad \omega = \sqrt{\frac{GM}{a^3}} \tag{27}$$

In the specific case the quantity $\frac{1}{2}(T_{AB} - T_{BA}) \approx 8.5 \times 10^{-7}$ s. This error is dominant over neglecting of $\delta t_{rel,AB}$ (which sits at or below the nanosecond-level), therefore we can assume that the magnitude of the largest error in the estimation of the actual offset is of the order of 1 μs. We can then safely assume that with such a coarse synchronization we are able to synchronize all satellites within a few microseconds.